Anticorrelation between electron-phonon coupling strength and stability of ternary metal diborides

Renhai Wang,[1,*] Feng Zheng,[2] Zhen Zhang,[3] Shunqing Wu,[4] Huafeng Dong,[1] Cai-Zhuang Wang,[3,5] Vladimir Antropov,[3,5,†] Yang Sun,[4,‡] and Kai-Ming Ho[3]

[1]*School of Physics and Optoelectronic Engineering, Guangdong University of Technology, Guangzhou 510006, China*
[2]*School of Science, Jimei University, Xiamen 361021, China*
[3]*Department of Physics and Astronomy, Iowa State University, Ames, Iowa 50011, USA*
[4]*Department of Physics, Xiamen University, Xiamen 361005, China*
[5]*Ames Laboratory-USDOE, Iowa State University, Ames, Iowa 50011, USA*

(Received 24 August 2024; revised 1 December 2024; accepted 23 December 2024; published 8 January 2025)

This paper endeavors to expand the exploration of prospective superconductivity within the $P6/mmm$-MgB_2 structural framework by substituting Mg atoms with a random selection of two distinct cations from a pool of 24 candidates. Employing a high-throughput screening methodology to scrutinize zone-center electron-phonon couplings, we found an inverse relationship between thermodynamic stability and electron-phonon coupling strength in the resulting ternary metal borides. Notably, within the $MgNiB_4$ system, we demonstrated that electron-phonon superconductivity is stronger in less dynamically stable configurations. The qualitative reasons for the emerging instabilities when electron-phonon coupling becomes strong are discussed. This insight indicates that the quest for superior superconducting materials should concentrate on the intricate balance between electronic and phononic characteristics in structures that are on the brink of instability.

DOI: 10.1103/PhysRevB.111.014104

I. INTRODUCTION

The appearance of different anomalies near the superconducting phase is commonly observed. The experimental evidence related to the connection between structural instability and superconductivity has been observed since the '60s and summarized in the review [1]. Theoretically, structural instability and superconductivity were discussed by Matthias [2], while Frolich [3] has shown that the superconducting interaction may cause instabilities in the phonon spectrum. Since then, the issue of instabilities in charge, spin, phonon, and lattice channels and their relation to superconductivity has been observed and discussed many times.

The simple reason for such instability can be seen already in the expression for the electron-phonon coupling (EPC) constant, λ [4]. Due to the direct proportionality of this quantity to the density of states at the Fermi level [$N(\epsilon_F)$], the simple recipe to increase superconducting critical temperature (T_c) would be to generate a material with the large $N(\epsilon_F)$. The studies of this effect and, in general, the behavior of electrons at the Fermi level (ϵ_F) are now termed fermiology, which plays an ultimate role in mechanisms of many different orderings. The presence of many electrons at the ϵ_F strongly affects the electronic subsystem's properties and interacts with all other properties.

Typically, large values of $N(\epsilon_F)$ simultaneously destroy the stability of the material, creating difficulties in their experimental synthesis. In some cases, losing initial stability is not a destructive factor, as it can transform the system into a stable magnetic, superconducting, or, for instance, charge density state [5–8]. Further increase of $N(\epsilon_F)$ would lead to the concept of flat bands [Van Hove singularities (VHS)], which play a crucial role in the topology of electronic and phonon band structures, including interactions with Kohn anomalies. The significance of such VHS becomes stronger in systems with lower dimensions [9,10], especially where spin fluctuations related to superconductivity are suspected. For instance, VHS in 2D materials has been a hot topic in many areas of solid-state physics, especially after discovering high-temperature superconductivity in cuprates [11] and many other superconductors. Anomalies at the ϵ_F were found actively participating in the properties of systems with phase separation and magnetic and charge instabilities [12–15]. Strong effects of large $N(\epsilon_F)$ were found in the anomalies of an anisotropic thermal expansion near points of electronic topological transition [16]. The impact of the proximity of the ϵ_F to VHS on the kinetic and lattice properties of metals and alloys was studied in Ref. [17].

The concept of EPC as a key factor in superconductivity is well-established. To delve deeper into this relationship and its implications for material stability, we focus on MgB_2 and its analogs. MgB_2, with its unique structure, serves as an ideal model system to explore how EPC interacts with and influences material stability. This class of structures provides a rich platform for understanding the intricate balance between superconducting properties and the thermodynamic stability of materials. So far, MgB_2 still holds the highest T_c in the conventionally superconducting materials under ambient conditions experimentally [18]. Multiple studies have indicated

*Contact author: wangrh@gdut.edu.cn
†Contact author: antropov@ameslab.gov
‡Contact author: yangsun@xmu.edu.cn

that the strong EPC in MgB_2 is associated with the peculiarities of chemical bonding [19,20]. Significant theoretical work has also been performed to replace the metal elements in the MgB_2 hexagonal structure. For instance, Yu *et al.* [21] used data-driven methods to study the superconductivity of a series of MgB_2-like structures and found that XB_2 (X = Mg, Al, Ca, Sc, V, Y, Nb, Ta), XSi_2 (X = Ca), XGa_2 (X = Sr, Ba), $BaAu_2$, and $LaCu_2$ are all superconductors. To find high-temperature superconductors with experimental synthesis potential in metal borides, theoretical research should simultaneously consider structural stability and superconducting properties.

In this paper, the high-throughput screening method of EPC [22] was used to expand the study of possible superconductivity in the MgB_2 structural framework by replacing 24 different metal atoms. We focus on computational analysis of the coexistence of thermodynamic stability and electron-phonon superconductivity in $MgNiB_4$-type systems and demonstrate that electron-phonon superconductivity in these systems is stronger in less stable materials. Thus, the search for better superconductors is naturally related to the delicate competition of electronic and phononic properties on the verge of structural instability.

II. COMPUTATIONAL METHODS

We initiated our computational approach by expanding the AlB_2-type primitive cell, belonging to the $P6/mmm$ space group, through a systematic $1 \times 1 \times 2$ or $2 \times 2 \times 1$ replication to construct the $M_{1-x}N_xB_2$ a ternary metal diboride frameworks, where M and N denote distinct metal elements. The variable x was assigned values of 0.25, corresponding to M_3NB_8, 0.50 for MNB_4, and 0.75 for M_3NB_8, respectively. From a pool of candidate structures, we meticulously selected those that were symmetry-inequivalent, yielding a single configuration for both M_3NB_8 and MN_3B_8, and two distinct configurations for MNB_4 (further details are available in Supplemental Material [23], Fig. S1).

The optimization of these ternary structures was conducted utilizing *ab initio* calculations, executed within the framework of density functional theory through the VASP code [24,25], employing the projector augmented wave method [26]. The exchange and correlation energies were calculated using the generalized gradient approximation in its spin-polarized form, parameterized by the Perdew-Burke-Ernzerhof formula [27]. A plane-wave basis set was engaged with a kinetic energy cutoff established at 520 eV, and the total energy convergence threshold was set to a stringent 10^{-5} eV. For the sampling of the Brillouin zone, we employed the Monkhorst-Pack scheme [28], following convergence tests, utilizing a k-point mesh density of $2\pi \times 0.033$ Å^{-1}. The lattice constants and atomic positions were fully optimized, with relaxation continuing until the forces exerted on each atom were diminished to below 0.01 eV/Å.

The formation energy E_f of ternary $M_xN_yB_z$ is calculated by

$$E_f = \frac{E(M_xN_yB_z) - xE(M) - yE(N) - zE(B)}{x+y+z}. \quad (1)$$

Here, $E(M_xN_yB_z)$ denotes the computed total energy of the $M_xN_yB_z$; while $E(M)$, $E(N)$, and $E(B)$ represent the total energies of the ground-state bulk phases of elements M, N, and B, respectively. To evaluate the thermodynamic stability, the formation energy above the convex hull (E_d) is computed. Considering that $M_xN_yB_z$ is dissociated by three reference phases ($M_{x_1}N_{y_1}B_{z_1}$, $M_{x_2}N_{y_2}B_{z_2}$, and $M_{x_3}N_{y_3}B_{z_3}$) of the Gibbs triangle on the convex hull, $M_xN_yB_z \rightarrow \alpha M_{x_1}N_{y_1}B_{z_1} + \beta M_{x_2}N_{y_2}B_{z_2} + \gamma M_{x_3}N_{y_3}B_{z_3}$, E_d can be calculated as follows:

$$E_d = \frac{E_f(M_xN_yB_z) - \alpha E_f\left(M_{x_1}N_{y_1}B_{z_1}\right) - \beta E_f\left(M_{x_2}N_{y_2}B_{z_2}\right) - \gamma E_f\left(M_{x_3}N_{y_3}B_{z_3}\right)}{x+y+z}. \quad (2)$$

We take $MgNiB_4$ as an example to clearly illustrate the calculation of E_d. As shown in Fig. S2, see Supplemental Material [23], we first construct the ternary Mg-Ni-B convex hull based on the reported stable phases. It can be seen that $MgNiB_4$ is situated within the Gibbs triangle composed of MgB_4, MgB_7, and $MgNi_3B_2$. Using the decomposition equation $MgNiB_4 \rightarrow (4MgB_4 + 2MgB_7 + 3MgNi_3B_2)/9$ and the above E_d calculation formula, it can be calculated that $E_d(MgNiB_4)$ is 0.18 eV/atom. The smaller the E_d, the more stable the system. The value of $E_d < 0$ indicates that $M_xN_yB_z$ represents a new ground state at 0 K and the existing convex hull needs to be updated. After the update, the E_d of all stable phases on the convex hull is 0 eV/atom. The references for these convex hulls were sourced from the Material Project dataset [29].

For the high-throughput screening of robust EPC in these metal borides, we employed a rapid frozen-phonon methodology to calculate the zone-center EPC strength [22], expressed as

$$\lambda_\Gamma = \sum_\nu \lambda_{\Gamma\nu}. \quad (3)$$

This summation encompasses all modes at the zone-center Γ, with $\lambda_{\Gamma\nu}$ defined as the ratio of the change in phonon frequency to the original unscreened frequency for mode ν,

$$\lambda_{\Gamma\nu} = \frac{\tilde{\omega}^2_{\Gamma\nu} - \omega^2_{\Gamma\nu}}{4\omega^2_{\Gamma\nu}}, \quad (4)$$

where the $\omega_{\Gamma\nu}$ and $\tilde{\omega}_{\Gamma\nu}$ are screened and unscreened phonon frequencies of mode ν, respectively. The phonon frequencies were obtained utilizing the single-cell finite displacement method within the PHONOPY code [30], applying a displacement amplitude of 0.02 Å for the frozen-phonon calculations. The total energy convergence criterion was set to 10^{-8} eV.

The estimation of λ_Γ can elucidate the relationship between the stability of our system and the strength of the EPC. To simplify, let us rewrite Eq. (4) in simplified form ignoring indices. We have (see also Eqs. (3.75) and (4.77) in Ref. [31])

$$\omega^2 = \tilde{\omega}^2 - 4\lambda\omega^2 = \tilde{\omega}^2 - 4\eta, \quad (5)$$

where η is the McMillan-Hopfield electronic stiffness (more often referred to as the Hopfield parameter [32]), characterizing the strength of electron-phonon interaction matrix elements. On the other hand, based on the electron-phonon coupling parameter formula $\lambda = 2N(\epsilon_F)\boldsymbol{g}^2/\omega$ [33,34], the

average value of the EPC matrix elements within the first Brillouin zone (1BZ), g^2, can be expressed as

$$g^2 = \frac{\eta}{2N(\epsilon_F)\omega}. \tag{6}$$

We conducted a comprehensive evaluation of the EPC constants across the entire Brillouin zone and the T_c for superconductivity in metal borides, leveraging the density-functional perturbation theory (DFPT) [35] as operationalized within the QUANTUM ESPRESSO code [36–38]. Our methodology incorporated ultrasoft pseudopotentials curated from the GBRV library [39], selected following rigorous convergence assessments. The computational parameters were meticulously calibrated, with a plane-wave energy cutoff and charge density cutoff set at 80 and 800 Ry, respectively.

In contrast to the structural relaxations performed with VASP, the calculation of electron-phonon coupling strengths using QUANTUM ESPRESSO required a denser k-point mesh to ensure convergence of the subtle phonon frequencies and electron-phonon matrix elements. For the MgB_2 reference system, utilizing the AlB_2-type primitive cell, we initiated our calculations with a self-consistent field (SCF) procedure employing a finely spaced k-point mesh of $48 \times 48 \times 48$. Subsequently, DFPT calculations were executed with a k-point grid of $24 \times 24 \times 24$ and a q-point grid of $6 \times 6 \times 6$, ensuring a robust quantum mechanical description of the system's properties. In the case of $MgNiB_4$, the calculations were predicated on a $1 \times 1 \times 2$ supercell, with the SCF calculations utilizing a dense k-point mesh of $48 \times 48 \times 24$. For the DFPT calculations, we employed a k-point mesh of $24 \times 24 \times 12$ and a q-point mesh of $6 \times 6 \times 3$, achieving a high level of computational accuracy with a convergence threshold of 1×10^{-15} Ry. Additionally, Gaussian smearing was applied with a width of 0.01 Ry to refine the electronic occupation statistics.

The isotropic Eliashberg spectral function was obtained by performing an average over the entirety of the Brillouin zone [40],

$$\alpha^2F(\omega) = \frac{1}{2N(\epsilon_F)} \sum_{q\nu} \frac{\gamma_{q\nu}}{\hbar\omega_{q\nu}} \delta(\omega - \omega_{q\nu}), \tag{7}$$

where $N(\epsilon_F)$ is the density of states (DOS) at the Fermi level ϵ_F. Additionally $\omega_{q\nu}$ signifies the phonon frequency for the mode ν with wave vector q. The phonon linewidth, $\gamma_{q\nu}$, is defined by $\gamma_{q\nu} = \frac{2\pi\omega_{q\nu}}{\Omega_{BZ}} \sum_{ij} \int d^3k |g^{ij}_{k,q\nu}|^2 \delta(\epsilon_{q,i} - \epsilon_F)\delta(\epsilon_{k+q,j} - \epsilon_F)$, where $g^{ij}_{k,q\nu}$ is the EPC matrix element; $\epsilon_{q,i}$ and $\epsilon_{k+q,j}$ are eigenvalues of Kohn-Sham orbitals at bands i, j, and wave vectors q, k. The integration of the Eliashberg spectral function yields the full Brillouin-zone EPC constant λ, expressed as

$$\lambda = \sum_{q\nu} \lambda_{q\nu} = 2 \int \frac{\alpha^2F(\omega)}{\omega} d\omega, \tag{8}$$

where the EPC constant $\lambda_{q\nu}$ for mode ν at wave vector q can be written as

$$\lambda_{q\nu} = \frac{\gamma_{q\nu}}{\pi\hbar N(\epsilon_F)\omega^2_{q\nu}}. \tag{9}$$

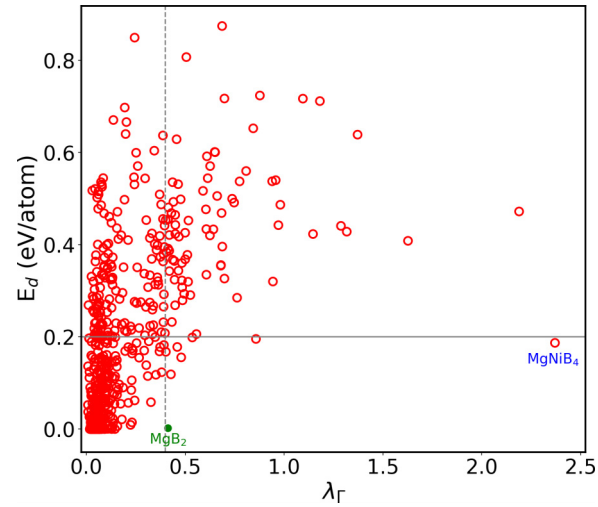

FIG. 1. E_d-λ_Γ diagram for ternary $M_{1-x}N_xB_2$ structures. The horizontal line indicates the range of energetic stability of synthesizable compounds. The vertical dashed line indicates λ_Γ value similar to MgB_2.

Subsequently, The T_c was deduced employing the analytical McMillan equation [41], refined by the Allen-Dynes modification [42,43], which accounts for the EPC and the effective screened Coulomb repulsion constant μ^*, assumed here to be 0.1. This equation is given by

$$T_c = \frac{\omega_{\log}}{1.2} \exp\left[\frac{-1.04(1+\lambda)}{\lambda(1-0.62\mu^*) - \mu^*}\right], \tag{10}$$

where $\omega_{\log}$ is the logarithmic average frequency $\omega_{\log} = \exp[\frac{2}{\lambda}\int \frac{d\omega}{\omega}\alpha^2F(\omega)\log\omega]$.

The Vickers hardness H_v was calculated using Chen's equation [44],

$$H_v = 2(\kappa^2G)^{0.585} - 3, \tag{11}$$

where $\kappa = \frac{G}{B}$, G is the shear moduli, and B is the bulk moduli.

III. RESULTS AND DISCUSSION

A. E_d-λ_Γ correlation in ternary $M_{1-x}N_xB_2$

The correlation between the E_d and λ_Γ (see the definition in the Methods section) for all examined ternary phases is delineated in Fig. 1, revealing a pronounced inverse relationship between the thermodynamic stability and EPC strength. In our high-throughput computational screening, we aim to streamline the experimental search for potential high-temperature superconductors, a process that is inherently slow and impractical to conduct for every possible system. Our approach efficiently identifies systems with strong electron-phonon coupling and favorable stability, providing a theoretical basis for experimental efforts. It is important to note that while the actual synthesis is influenced by various external factors and is beyond the scope of this paper, several d-electron containing ternary metal diborides, such as $Mg_{0.75}Sc_{0.25}B_2$ and $Zr_{1-x}Nb_xB_2$ ($x = 0.25, 0.5, 0.75$), have been successfully synthesized. These examples affirm the potential for experimental realization of systems similar to those identified in our paper, highlighting the practical implications of our

TABLE I. Crystallographic data of α-$MgNiB_4$ and γ-$MgNiB_4$

Phase	λ_Γ	E_f (eV/atom)	Lattice parameter	Atom	x	y	z
α-$MgNiB_4$	2.37	−0.033	$a = b = 3.026$ Å	Mg	0	0	0.5
			$c = 6.508$ Å	Ni	0	0	0
			$\alpha = \beta = 90°, \gamma = 120°$	B	0.333	0.667	0.229
γ-$MgNiB_4$	0.33	−0.036	$a = b = 3.018$ Å	Mg	0.988	0.977	0.5
			$c = 6.531$ Å	Ni	0.029	0.057	0
			$\alpha = \beta = 90°, \gamma = 120°$	B	0.333	0.667	0.228

theoretical predictions for guiding future experimental research. Our screening for phases with synthetic potential, informed by literature research, identified numerous metastable states with E_d around 0.2 eV/atom that can be synthesized via nonequilibrium pathways. For instance, the $Li_{0.75}NiB_2$ phase with $E_d = 0.21$ eV/atom [45], $SnTi_2N_4$ with $E_d = 0.2$ eV/atom [46], and $ZnMoN_2$ with $E_d = 0.16$ eV/atom [47] are notable examples. Utilizing a criterion of $E_d < 0.2$ eV/atom, we have identified structures that exhibit commendable stability, as illustrated in Fig. 1. Furthermore, by applying a λ_Γ threshold of approximately 0.4, akin to that observed in MgB_2, we have effectively filtered structures that demonstrate robust EPC. Notably, the ternary phases that meet both of these stringent criteria are situated in the lower-right quadrant of Fig. 1, with $MgNiB_4$ (named α-$MgNiB_4$) emerging as the phase with the most pronounced EPC strength, boasting a λ_Γ value of 2.37.

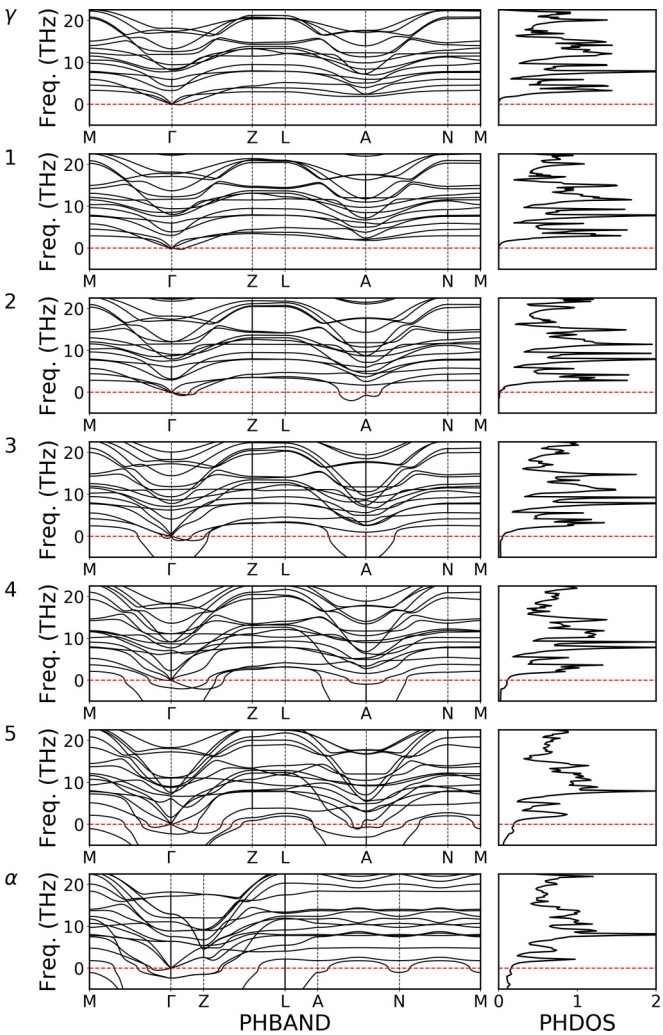

FIG. 2. Phonon spectrum and phonon state density from γ-$MgNiB_4$ to α-$MgNiB_4$.

Delving deeper into the case of $MgNiB_4$, we embarked on a detailed investigation to elucidate the interplay between structural stability and EPC. Our initial assessment of the phonon spectrum and state density for the α-$MgNiB_4$ phase, characterized by a strong initial EPC, revealed the presence of a significant imaginary frequency [as shown in Fig. 2]. This observation is indicative of the potential for a lower energy configuration. Through the strategic elimination of imaginary frequencies, we successfully uncovered a unique dynamically stable structure, designated as γ-$MgNiB_4$, which exhibits a reduced energy state and enhanced dynamic stability. Comparatively, the lattice parameters for this phase have undergone subtle adjustments: a and b have contracted by 2.6%, while c has expanded by 3.5%, as detailed in Table I. Most notably, the Mg and Ni atoms in γ-$MgNiB_4$ have been found to deviate from their original positions by a minor extent, yet in opposite directions, as visualized in Fig. 3.

Subsequently, our calculations targeted the EPC strength λ_Γ of the γ-$MgNiB_4$ phase, yielding a value of 0.33, indicative of a noteworthy reduction of approximately 86% compared to the α-$MgNiB_4$ phase. This prompted an inquiry into the underpinnings of the diminished EPC. To this end, we strategically interposed five intermediate structures (named 1, 2, 3, 4, and 5) between γ-$MgNiB_4$ and α-$MgNiB_4$, facilitating a gradual transition from the former to the latter. Figure 2 presents the phonon spectra and state densities for these intermediate structures, indicating that the imaginary frequency increases continuously from the stable phase γ to the unstable phase α.

Further elucidation was provided by Fig. 4, which delineates the transformation in electronic band structures and

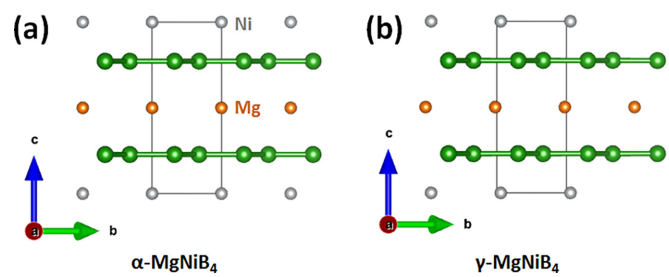

FIG. 3. Structure snapshot of (a) α-$MgNiB_4$ and (b) γ-$MgNiB_4$.

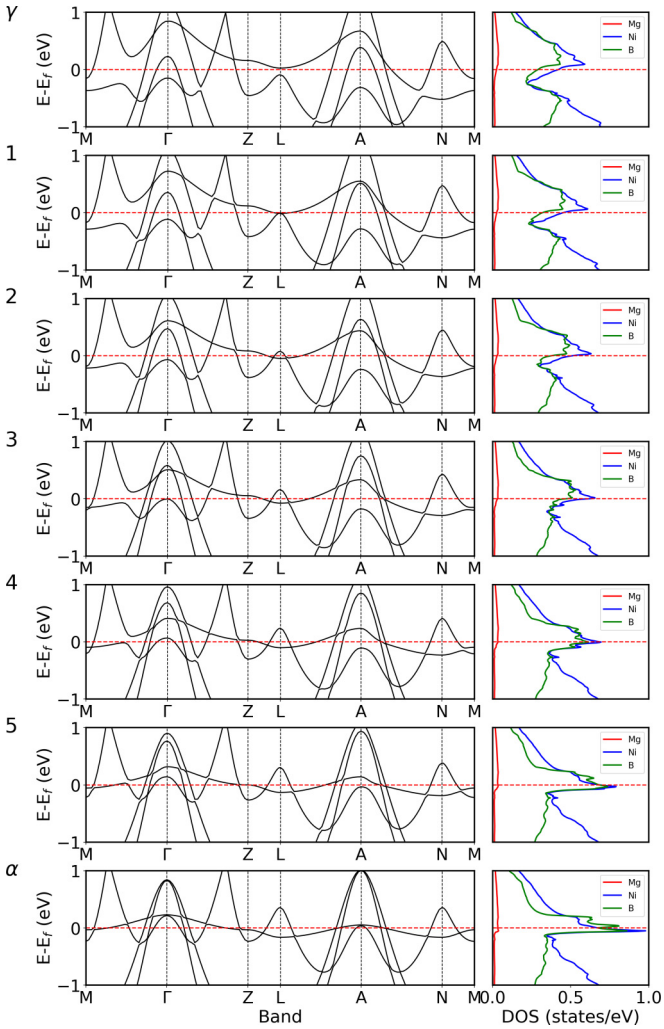

FIG. 4. Energy bands and density of states from γ-$MgNiB_4$ to α-$MgNiB_4$.

DOS across the γ-$MgNiB_4$ to α-$MgNiB_4$ continuum. A discernible increment in $N(\epsilon_F)$ is observed, culminating in a pronounced peak for α-$MgNiB_4$. This sharp feature is the harbinger of the robust EPC characteristic of this phase. However, as we discussed in the Introduction, large $N(\epsilon_F)$ leads to possible development of instabilities in other channels making overall stability questionable.

Our estimation of zone-center electron-phonon couplings λ_Γ can also be used to illustrate how the stability of our systems (Figs. 1 and 2) can be related to the strength of EPC. Considering the Hopfield parameter η from Eq. (5) (see Methods), for a family of similar materials as discussed here, one can assume that η is changing little. However, such an assumption of constant η has been found unjustified in several classes of materials, including hydrides [48]. Thus, when η is increasing, the electronic screening of phonon frequencies becomes so large that resulting phonons obtain imaginary parts and the system becomes dynamically unstable. This simple consideration clearly demonstrates the natural appearance of instabilities when electron-phonon coupling increases. In turn, it could lead to the appearance of different types of structural transitions. To substantiate this assertion, we have delineated the trajectories of η, $\boldsymbol{g}^2$, and λ throughout the transition of $MgNiB_4$ from the stable to the unstable phase, as depicted in Fig. 5. It is evident that, for the majority of the modes, both η and $\boldsymbol{g}^2$ exhibit consistent behavior with the trajectories of λ. As instability emerges, all three parameters escalate, corroborating the aforementioned qualitative exposition.

Based on such consideration, the next evident opportunity for higher T_c is to find other materials with very low $\tilde{\omega}^2$. This direction has two fundamental limitations: structures with such low $\tilde{\omega}^2$ tend not to be stable, and the fact when the EPC lambda is increasing due to low $\tilde{\omega}^2$, the resulting T_c begins to go up rather slow for $\lambda > 1$. A progress in this direction can be expected by generating metastable materials with very low $\tilde{\omega}^2$. Another opportunity for T_c increase would be direct change of the Hopfield parameter by changing the type of bonding (with the corresponding change of $\tilde{\omega}^2$) and considering high atomic density systems. Increasing η would increase $\tilde{\omega}^2$ also, as both are proportional to the squared matrix element of forces. But averages involved in these two quantities are different and this difference could allow for λ to be higher (see Fig. 5). Materials with exotic dependence of η on Fermi surface wave functions would also produce different from normal values of λ as well.

The case study of $MgNiB_4$ illustrates a pivotal trade-off: while enhancements in the thermodynamic stability of a material are conducive to bolstering its dynamic stability, they concurrently result in a diminution of the EPC strength. This inverse relationship has profound implications for the superconducting properties of the material, suggesting that the pursuit of stability may come at the expense of optimal superconducting performance. The qualitative discussion above can be used for the discussion of stability in spin-fluctuation-induced superconducting systems like cuprates or pnictides.

B. Superconductivity in $M_{1-x}N_xB_2$

Given the auspicious synthesizability and EPC potential of the γ-$MgNiB_4$ phase, we performed DFPT calculations to meticulously determine the full Brillouin zone EPC constant. Subsequently, we harnessed the McMillan equations, as detailed in our methodology, to calculate the T_c for superconductivity. The phonon spectrum and the density of states for the γ-$MgNiB_4$ phase are displayed in Fig. 6(a). The absence of any imaginary-frequency modes along the high-symmetry lines of the Brillouin zone suggests its dynamic stability of γ-$MgNiB_4$. The EPC constant of γ-$MgNiB_4$ is $\lambda = 0.60$. Employing a consistent approach and maintaining the same density of k- and q-grid points as outlined in the Methods section, we obtained the T_c of 11.7 K for γ-$MgNiB_4$, which is approximately half that of the renowned MgB_2 superconductor (22.9 K) [49]. Despite the reduced T_c, the discovery of $MgNiB_4$ with enhanced stability and moderate superconductivity offers a promising direction for the development of new superconducting materials with a balance of desirable properties.

We compared the phonon dispersion, phonon density of states, and Eliashberg spectra of MgB_2 and γ-$MgNiB_4$, as shown in Fig. 6. Our analysis reveals that the $\alpha^2F(\omega)$ peak of MgB_2 corresponds primarily to the high-frequency phonon modes of boron atoms, which contribute significantly to the electron-phonon coupling strength. In contrast, the $\alpha^2F(\omega)$

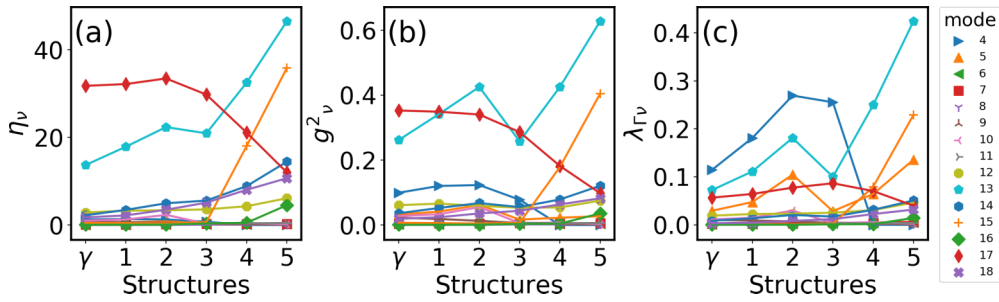

FIG. 5. The variation of (a) η, (b) g^2, and (c) λ as $MgNiB_4$ structures transition from the stable phase to unstable phase. The horizontal axis labels, γ, 1, 2, 3, 4, and 5, correspond to the structural names depicted in Figs. 2 and 4; the different symbols in the legend represent the 15 optical branch modes within the $MgNiB_4$ structure.

peak of $MgNiB_4$ is more broadly distributed, encompassing both the low-frequency phonon modes of Ni and the mid- to high-frequency phonon modes of B. Notably, Ni atoms contribute approximately 40% to the electron-phonon coupling, which leads to a reduction in the overall electron-phonon coupling strength of the system. Additionally, there is a noticeable decrease in the logarithmic average frequency, $\omega_{\log}$, from 700 K in MgB_2 to 399 K in $MgNiB_4$, suggesting that the introduction of the $3d$ electron metal atom Ni inhibits the λ and T_c of the MgB_2-like structure.

Our previous studies have demonstrated that rapid EPC calculations can effectively suggest potential conventional superconductors for future experimental research [22,50]. Here, by comparing the full Brillouin zone DFPT-calculated EPC constants (λ_{BZ}) with the zone-center EPC strength for systems containing d-electrons (see Table II), we found a considerably positive correlation, as shown in Fig. S3, see Supplemental Material [23]. For most systems, a significant λ_Γ corresponds to a high λ_{BZ}, and many systems exhibit T_c values above that of MgB_2. This is because, as observed from the phonon dispersion in Figs. S4–S10, see Supplemental Material [23], the contributions to EPC across the high-symmetry points in the Brillouin zone are relatively dispersed, while in MgB_2, the EPC is mainly derived from the Γ to A path. The

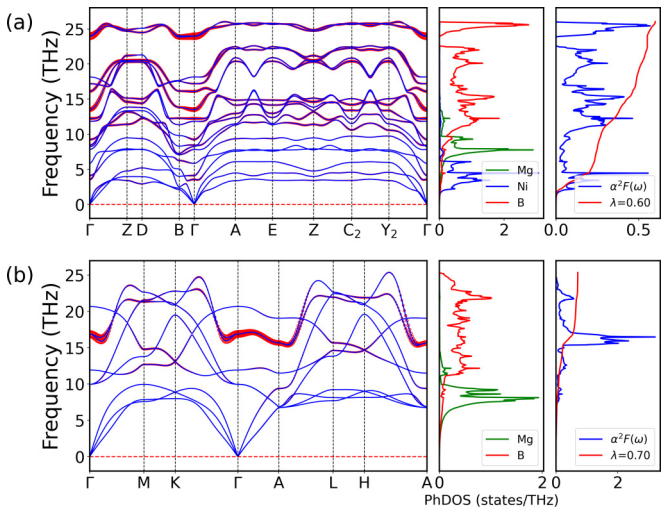

FIG. 6. Phonon dispersion, phonon density of states, and Eliashberg spectrum of (a) γ-$MgNiB_4$ and (b) MgB_2. The red bands on the phonon dispersion indicate the strength of the phonon linewidth.

mixing of d states will indeed alter the contribution of other phonons to electron-phonon coupling. Nonetheless, using the electron-phonon coupling signal at the Γ point to screen for high-temperature superconducting systems, including those with d electrons, remains an effective method.

C. E_d-metal correlation in ternary $M_{1-x}N_xB_2$

The intricate relationship between E_d and the metal constituents in ternary $M_{1-x}N_xB_2$ systems is shown in Fig. 7. Each grid within this figure is color-coded to correspond to the E_d value of the respective phase, with darker shades of blue indicating greater energetic stability. For comparative purposes, the binary phase data are strategically positioned along the diagonal, serving as a benchmark for analysis.

An observation emanating from this visualization is the inverse correlation between the number of d electrons in the transition metals and the thermodynamic stability of the resulting metal borides. Phases incorporating transition metals with a reduced d-electron count exhibit a heightened propensity for stable formation. This insight is valuable, as it enlightens our approach to the synthesis of advanced ternary or even quaternary metal borides. Specifically, it suggests that the judicious selection of transition metals with fewer d electrons in their outer shell could be a key strategy to enhance the stability of these complex materials.

TABLE II. Superconducting properties of dynamically stable systems containing d-electron elements. λ_Γ represents the results of the electron-phonon coupling obtained from the rapid zone-center calculations, while λ_{BZ} denotes the EPC results derived from the full Brillouin zone calculations.

System	λ_Γ	λ_{BZ}	T_c (K)
MgB_2	0.41	0.70	22.9
$MgNiB_4$	0.33	0.60	11.7
Li_3ZrB_8	0.37	1.04	38.0
Ca_3YB_8	0.39	0.64	10.0
Li_3ScB_8	0.29	0.90	31.1
$LiZn_3B_8$	0.24	0.89	28.6
Na_3ScB_8	0.36	0.88	29.4
Na_3ZrB_8	0.48	1.05	34.3
Y_3CdB_8	0.19	0.37	1.3
Cd_3ScB_8	0.32	0.58	10.8
Ca_3ZrB_8	0.18	0.50	5.4

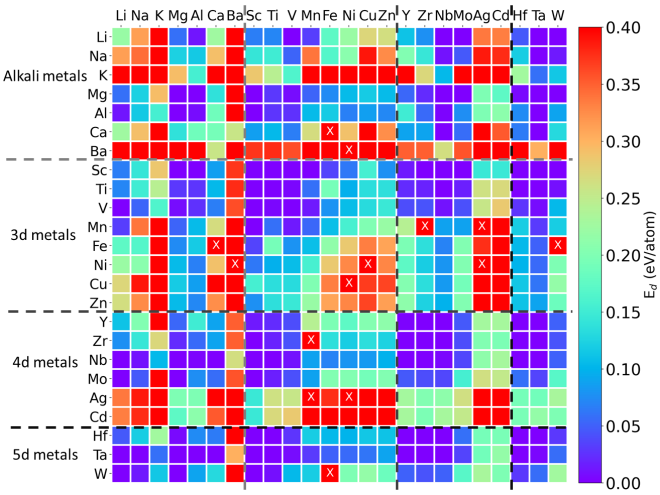

FIG. 7. E_d mapping of ternary metal diboride compounds, with darker shades of blue indicating greater energetic stability. X axis indicates N site and Y axis indicates M site.

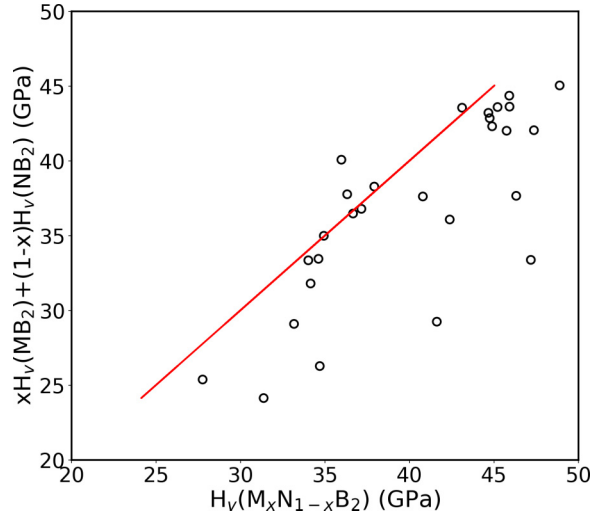

FIG. 8. The comparison between the H_v of ternary phases and the linear combinations of their binary counterparts. The x axis shows the value of ternary phases, i.e., $H_v(M_{1-x}N_xB_2)$. The y axis shows the linear combination of the binary counterparts, i.e., $(1-x)H_v(MB_2)+xH_v(NB_2)$. The red line indicates $y=x$ correlation.

D. Vickers hardness of stable $M_{1-x}N_xB_2$

Our investigation has identified an abundance of thermodynamically stable ternary metal borides, prominently featured in the lower left section of Fig. 1. These compounds hold considerable promise for experimental synthesis. Among these, we have selected a subset of structures and proceeded to calculate their Vickers hardness, a metric that quantifies the resistance of a material to indentation. The results, as compiled in Table S1 (see Supplemental Material [23]), reveal that a majority of these structures exhibit commendable hardness.

To understand the cation mixing effect in the ternary phase, we recalculate the H_v value by linear interpolation between the binary phases [illustrated by the formula $H_v(M_{1-x}N_xB_2)=(1-x)H_v(MB_2)+xH_v(NB_2)$] and compare the calculated values with the actual values in Fig. 8. It can be seen that H_v in Fig. 8 strongly deviates from the $y=x$ line. A substantial number of ternary phases demonstrate superior Vickers hardness compared to the linear combinations of their constituent binary parent phases. This enhancement may be attributed to electronic effects that alter bonding characteristics or geometrical relaxation effects. Our findings indicate that cation mixing is an effective strategy to enhance the hardness of binary materials. However, only two specific ternary phases, Zr_3TaB_8 and Hf_3TaB_8, which both contain Ta, exhibit a weakening of H_v (above the $y=x$ line), as shown in Fig. S11(a); see Supplemental Material [23].

To unravel the physical reasons behind the anomalies in these two systems, we conducted a comparison of the bulk modulus (B), shear modulus (G), and volume (V) for all ternary systems with their binary linear interpolations, as shown in Figs. S11(b)– S11(d); see Supplemental Material [23]. It is evident that only the G and H_v consistently exhibit behavior above the $y=x$ line. According to Chen's formula for calculating Vickers hardness [see Eq. (11)], the value of G substantially influences H_v. Generally, a higher shear modulus is associated with stronger atomic bonds within layered structures, as these strong bonds are more resistant to shear deformation. So, we compared the systems containing Ta elements above the $y=x$ line (Zr_3TaB_8, Hf_3TaB_8) with those below the line (Sc_3TaB_8, Ti_3TaB_8). Table S2 (see Supplemental Material [23]) lists the B–B bond lengths adjacent to Ta in these systems, in contrast to the binary TaB_2. It is clear that the B–B bond lengths in the systems below the $y=x$ line are shorter, indicating stronger bonds, while those above the line are longer, suggesting weaker bonds. This results in a decreased shear modulus and, consequently, a reduced Vickers hardness for the systems positioned above the line.

IV. CONCLUSION

In summary, our high-throughput first-principles calculations have shed light on the interplay between thermodynamic stability and EPC strength across a spectrum of ternary systems involving alkali metals, alkaline earth metals, $3d$, $4d$, and $5d$ transition metals in diboride compounds. The phonon spectrum and electronic density of states analysis of $MgNiB_4$ have unveiled the inverse relationship between energy stability and EPC strength. The dynamically stable ternary phases Li_3ScB_8, $LiZn_3B_8$, Na_3ScB_8, and Na_3ZrB_8 exhibit critical temperatures that surpass that of MgB_2. Furthermore, our examination of the thermodynamic stability of transition metal borides has revealed that transition metals with a reduced count of d electrons are instrumental in the formation of multielement metal borides. We qualitatively discuss the reasons for developed instabilities in the superconducting systems when electron-phonon interactions become stronger. These insights guide our future exploration toward materials that possess robust EPC, potentially residing on the cusp of instability, as promising candidates for the next generation of superconductors.

ACKNOWLEDGMENTS

Work at Guangdong University of Technology was supported by the Guangdong Basic and Applied Basic Research Foundation (Grants No. 2021A1515110328 and No. 2022A1515012174). Y.S. was supported by the National Natural Science Foundation of China (Grants No. T2422016 and No. 42374108), the Natural Science Foundation of Xiamen (Grant No. 3502Z202371007), and the Fundamental Research Funds for the Central Universities (Grant No. 20720230014). R.W. was supported by the Guangdong University of Technology SPOE Seed Foundation (Grant No. SF2024111506). F.Z. was supported by the National Natural Science Foundation of China (Grant No. 12404077), the Natural Science Foundation of Xiamen Municipality (Grant No. 3502Z202372015) and the Research Foundation of Jimei University (Grant No. ZQ2023013). S.W. was supported by the National Natural Science Foundation of China (11874307). C.Z.W. and V.A. were supported by the U.S. Department of Energy (DOE), Office of Science, Basic Energy Sciences, Materials Science and Engineering Division. Ames Laboratory is operated for the U.S. DOE by Iowa State University under Contract No. DE-AC02-07CH11358, including the grant of computer time at the National Energy Research Supercomputing Center (NERSC) in Berkeley. R.W. and H.D. also thank the Center of Campus Network and Modern Educational Technology of GDUT for providing computational resources and technical support for this work.

[1] L. Testardi, Structural instability and superconductivity in A-15 compounds, Rev. Mod. Phys. **47**, 637 (1975).

[2] B. Matthias, *Superconductivity in D-and F-Band Metals* (American Institute of Physics, New York, 1972), Vol. 367.

[3] H. Fröhlich, Superconductivity, lattice stability and phonon frequencies, Phys. Lett. A **35**, 325 (1971).

[4] V. Meregalli and S. Y. Savrasov, Electron-phonon coupling and properties of doped $BaBiO_3$, Phys. Rev. B **57**, 14453 (1998).

[5] M. Fleck, A. M. Oleś, and L. Hedin, Magnetic phases near the van hove singularity in *s*-and *d*-band Hubbard models, Phys. Rev. B **56**, 3159 (1997).

[6] J. Gonzalez, Kohn-Luttinger superconductivity in graphene, Phys. Rev. B **78**, 205431 (2008).

[7] W. Kohn and J. Luttinger, New mechanism for superconductivity, Phys. Rev. Lett. **15**, 524 (1965).

[8] T. Rice and G. Scott, New mechanism for a charge-density-wave instability, Phys. Rev. Lett. **35**, 120 (1975).

[9] G. Li, A. Luican, J. Lopes dos Santos, A. Castro Neto, A. Reina, J. Kong, and E. Andrei, Observation of Van Hove singularities in twisted graphene layers, Nat. Phys. **6**, 109 (2010).

[10] W. Wan, R. Harsh, P. Dreher, F. de Juan, and M. M. Ugeda, Superconducting dome by tuning through a Van Hove singularity in a two-dimensional metal, npj 2D Mater. Appl. **7**, 41 (2023).

[11] E. Dagotto, A. Nazarenko, A. Moreo, S. Haas, and M. Boninsegni, A simple theory for the cuprates: The antiferromagnetic Van Hove scenario, J. Supercond. **8**, 483 (1995).

[12] J. Bok and J. Bouvier, Van Hove scenario for high T_c superconductors, in *High T_c Superconductors and Related Transition Metal Oxides*, Special Contributions in Honor of K. Alex Müller on the Occasion of his 80th Birthday, Vol. 35 (Springer, Berlin, Heidelberg, 2007).

[13] V. Y. Irkhin, A. A. Katanin, and M. I. Katsnelson, Effects of Van Hove singularities on magnetism and superconductivity in the $t - t'$ Hubbard model: A parquet approach, Phys. Rev. B **64**, 165107 (2001).

[14] W. F. Goh and W. E. Pickett, A mechanism for weak itinerant antiferromagnetism: Mirrored Van Hove singularities, Europhys. Lett. **116**, 27004 (2016).

[15] Y. Sun, Z. Zhang, A. P. Porter, K. Kovnir, K.-M. Ho, and V. Antropov, Prediction of Van Hove singularity systems in ternary borides, npj Comput. Mater. **9**, 204 (2023).

[16] V. Antropov, M. Katsnelson, V. Koreshkov, A. Likhtenstein, A. Trefilov, and V. Vaks, On anomalies of anisotropic thermal expansion near points of electronic topological transitions in noncubic metals. applications to Zn, Cd and Cd-Mg alloys, Phys. Lett. A **130**, 155 (1988).

[17] V. Antropov, V. G. Vaks, M. I. Katsnel'son, V. G. Koreshkov, A. Likhtenshteĭn, and A. Trefilov, Effect of proximity of the fermi level to singular points in the band structure on the kinetic and lattice properties of metals and alloys, Sov. Phys. Usp. **31**, 278 (1988).

[18] J. Nagamatsu, N. Nakagawa, T. Muranaka, Y. Zenitani, and J. Akimitsu, Superconductivity at 39 K in magnesium diboride, Nature (London) **410**, 63 (2001).

[19] K. D. Belashchenko, M. van Schilfgaarde, and V. P. Antropov, Coexistence of covalent and metallic bonding in the boron intercalation superconductor MgB_2, Phys. Rev. B **64**, 092503 (2001).

[20] I. Mazin and V. Antropov, Electronic structure, electron–phonon coupling, and multiband effects in MgB_2, Physica C: Superconductivity **385**, 49 (2003).

[21] Z. Yu, T. Bo, B. Liu, Z. Fu, H. Wang, S. Xu, T. Xia, S. Li, S. Meng, and M. Liu, Superconductive materials with MgB_2-like structures from data-driven screening, Phys. Rev. B **105**, 214517 (2022).

[22] Y. Sun, F. Zhang, C.-Z. Wang, K.-M. Ho, I. I. Mazin, and V. Antropov, Electron-phonon coupling strength from *ab initio* frozen-phonon approach, Phys. Rev. Mater. **6**, 074801 (2022).

[23] See Supplemental Material at http://link.aps.org/supplemental/10.1103/PhysRevB.111.014104 for four symmetry-inequivalent crystal structures; convex hull of the Mg-Ni-B system; a scatter plot of λ_Γ versus λ_{BZ}; phonon dispersion, phonon density of state and Eliashberg spectrum of dynamically stable ternary metal diborides containing *d*-electron metal elements; the comparison between the H_v, B, G, V of ternary phases and the linear combinations of their binary counterparts; the calculated Vickers hardness value H_v; the B-B bond lengths adjacent to Ta in Ta-containing metal diboride systems.

[24] G. Kresse and J. Furthmüller, Efficiency of ab-initio total energy calculations for metals and semiconductors using a plane-wave basis set, Comput. Mater. Sci. **6**, 15 (1996).

[25] G. Kresse and J. Furthmüller, Efficient iterative schemes for ab initio total-energy calculations using a plane-wave basis set, Phys. Rev. B **54**, 11169 (1996).

[26] P. E. Blöchl, Projector augmented-wave method, Phys. Rev. B **50**, 17953 (1994).
[27] J. P. Perdew, K. Burke, and M. Ernzerhof, Generalized gradient approximation made simple, Phys. Rev. Lett. **77**, 3865 (1996).
[28] H. J. Monkhorst and J. D. Pack, Special points for Brillouin-zone integrations, Phys. Rev. B **13**, 5188 (1976).
[29] A. Jain, S. P. Ong, G. Hautier, W. Chen, W. D. Richards, S. Dacek, S. Cholia, D. Gunter, D. Skinner, G. Ceder *et al.*, Commentary: The materials project: A materials genome approach to accelerating materials innovation, APL Mater. **1**, 011002 (2013).
[30] A. Togo and I. Tanaka, First principles phonon calculations in materials science, Scr. Mater. **108**, 1 (2015).
[31] V. L. Ginzburg and D. A. E. Kirzhnits, *Problema Vysokotemperaturnoi Sverkhprovodimosti—the Problem of High-Temperature Superconductivity* (Moscow, Nauka, Moscow, 1977) [Translated into English: *High-Temperature Superconductivity* (Consultants Bureau, New York, 1982)].
[32] J. J. Hopfield, Angular momentum and transition-metal superconductivity, Phys. Rev. **186**, 443 (1969).
[33] M. Alidoosti, D. N. Esfahani, and R. Asgari, Superconducting properties of doped blue phosphorene: effects of non-adiabatic approach, 2D Mater. **9**, 045029 (2022).
[34] M. Alidoosti, D. N. Esfahani, and R. Asgari, Charge density wave and superconducting phase in monolayer InSe, Phys. Rev. B **103**, 035411 (2021).
[35] S. Baroni, S. De Gironcoli, A. Dal Corso, and P. Giannozzi, Phonons and related crystal properties from density-functional perturbation theory, Rev. Mod. Phys. **73**, 515 (2001).
[36] P. Giannozzi, S. Baroni, N. Bonini, M. Calandra, R. Car, C. Cavazzoni, D. Ceresoli, G. L. Chiarotti, M. Cococcioni, I. Dabo *et al.*, QUANTUM ESPRESSO: A modular and open-source software project for quantum simulations of materials, J. Phys.: Condens. Matter **21**, 395502 (2009).
[37] P. Giannozzi, Jr., O. Andreussi, T. Brumme, O. Bunau, M. B. Nardelli, M. Calandra, R. Car, C. Cavazzoni, D. Ceresoli, M. Cococcioni *et al.*, Advanced capabilities for materials modelling with QUANTUM ESPRESSO, J. Phys.: Condens. Matter **29**, 465901 (2017).
[38] P. Giannozzi, O. Baseggio, P. Bonfà, D. Brunato, R. Car, I. Carnimeo, C. Cavazzoni, S. de Gironcoli, P. Delugas, F. Ferrari Ruffino, A. Ferretti, N. Marzari, I. Timrov, A. Urru, and S. Baroni, QUANTUM ESPRESSO toward the exascale, J. Chem. Phys. **152**, 154105 (2020).
[39] K. F. Garrity, J. W. Bennett, K. M. Rabe, and D. Vanderbilt, Pseudopotentials for high-throughput DFT calculations, Comput. Mater. Sci. **81**, 446 (2014).
[40] G. Eliashberg, Interactions between electrons and lattice vibrations in a superconductor, J. Exptl. Theoret. Phys. **38**, 966 (1960) [Sov. Phys. JETP **11**, 696 (1960)].
[41] W. McMillan, Transition temperature of strong-coupled superconductors, Phys. Rev. **167**, 331 (1968).
[42] P. B. Allen, Neutron spectroscopy of superconductors, Phys. Rev. B **6**, 2577 (1972).
[43] P. B. Allen and R. Dynes, Transition temperature of strong-coupled superconductors reanalyzed, Phys. Rev. B **12**, 905 (1975).
[44] X.-Q. Chen, H. Niu, D. Li, and Y. Li, Modeling hardness of polycrystalline materials and bulk metallic glasses, Intermetallics **19**, 1275 (2011).
[45] G. Bhaskar, V. Gvozdetskyi, M. Batuk, K. M. Wiaderek, Y. Sun, R. Wang, C. Zhang, S. L. Carnahan, X. Wu, R. A. Ribeiro *et al.*, Topochemical deintercalation of Li from layered LiNiB: Toward 2D MBene, J. Am. Chem. Soc. **143**, 4213 (2021).
[46] A. Bikowski, S. Siol, J. Gu, A. Holder, J. S. Mangum, B. Gorman, W. Tumas, S. Lany, and A. Zakutayev, Design of metastable tin titanium nitride semiconductor alloys, Chem. Mater. **29**, 6511 (2017).
[47] E. Arca, S. Lany, J. D. Perkins, C. Bartel, J. Mangum, W. Sun, A. Holder, G. Ceder, B. Gorman, G. Teeter *et al.*, Redox-mediated stabilization in zinc molybdenum nitrides, J. Am. Chem. Soc. **140**, 4293 (2018).
[48] Y. Quan, S. S. Ghosh, and W. E. Pickett, Compressed hydrides as metallic hydrogen superconductors, Phys. Rev. B **100**, 184505 (2019).
[49] R. Wang, Y. Sun, F. Zhang, F. Zheng, Y. Fang, S. Wu, H. Dong, C.-Z. Wang, V. Antropov, and K.-M. Ho, High-throughput screening of strong electron–phonon couplings in ternary metal diborides, Inorg. Chem. **61**, 18154 (2022).
[50] S. Chen, Z. Wu, Z. Zhang, S. Wu, K.-M. Ho, V. Antropov, and Y. Sun, High-throughput screening for boride superconductors, Inorg. Chem. **63**, 8654 (2024).